Transformations in methane hydrates

I-Ming Chou*†, Anurag Sharma‡, Robert C. Burruss§, Jinfu Shu‡, Ho-kwang Mao‡, Russell J. Hemley‡, Alexander F. Goncharov‡, Laura A. Stern¶, and Stephen H. Kirby¶

*954 National Center and §956 National Center, United States Geological Survey, Reston, VA 20192; ‡Geophysical Laboratory and Center for High Pressure Research, Carnegie Institution of Washington, 5251 Broad Branch Road, NW, Washington, DC 20015; and ¶MS/977 United States Geological Survey, Menlo Park, CA 94025

Contributed by Ho-kwang Mao, October 2, 2000

Detailed study of pure methane hydrate in a diamond cell with *in situ* optical, Raman, and x-ray microprobe techniques reveals two previously unknown structures, structure II and structure H, at high pressures. The structure II methane hydrate at 250 MPa has a cubic unit cell of $a = 17.158(2)$ Å and volume $V = 5051.3(13)$ Å^3; structure H at 600 MPa has a hexagonal unit cell of $a = 11.980(2)$ Å, $c = 9.992(3)$ Å, and $V = 1241.9(5)$ Å^3. The compositions of these two investigated phases are still not known. With the effects of pressure and the presence of other gases in the structure, the structure II phase is likely to dominate over the known structure I methane hydrate within deep hydrate-bearing sediments underlying continental margins.

At moderately high pressures and low temperatures, methane gas can be trapped and stabilized by water in a solid form known as methane hydrate. With the immense reserve of methane hydrate in marine sediments (1), methane's significance as a greenhouse gas implicated in global climate issues and as a potential major energy resource has been widely recognized. In pure water, different arrangements of the tetrahedrally coordinated oxygen atoms and variable hydrogen bond lengths and angles result in a remarkable number of ice phases (2, 3). Insertion of various guest molecules in structural cavities of the H_2O polyhedral frameworks stabilizes at least 10 more structures, which fall into three archetypes of gas hydrate: structure I (sI), structure II (sII), and structure H (sH) (4–6). Pure methane hydrate, by far the most terrestrially abundant gas hydrate, is known to form only the cubic sI, in which both large and small cavities comfortably accommodate the small methane molecules. Applying pressure and performing *in situ* characterization, we have discovered the existence of two additional forms (sII and sH) of pure methane hydrate that are stable at higher pressures and temperatures than sI.

In mixed-gas hydrates containing methane in the small cavities, larger molecules such as propane or isobutane are normally required to stabilize the large H_2O cavities in sII, and even larger molecules such as isopentane and neohexane are needed to stabilize the larger cavities in sH (7). The formation of sII hydrate from mixtures of sI-formers, such as methane and ethane, has also been predicted (7) and demonstrated by recent Raman and NMR spectroscopic observations (8, 9). In pure methane hydrate, previous high-pressure studies that used differential thermal analysis methods revealed a phase transition above 500 MPa (Fig. 1), but the nature of the additional phase (or phases) was not determined (11, ‖). In contrast, other investigators (16) obtained polycrystalline x-ray diffraction measurements at 200 to 5,500 MPa, which they interpreted to indicate that methane hydrate maintains the sI with changes only in cavity occupancy.

In the present study, synthetic sI methane hydrate (17) was loaded in the sample chamber of a diamond cell (18). We found that methane hydrate transforms to a phase with different optical appearance and Raman signature at about 100 MPa (I-M.C., A.S., R.C.B., R.J.H., A.F.G., L.A.S., and S.H.K., unpublished observations). As shown by the single-crystal x-ray diffraction data presented below, this phase is no longer sI, but a methane hydrate with sII characteristics. When compressed to higher pressures, a different phase (Fig. 2*a*; sH, as discussed below) appeared at about 600 MPa. Although the characteristic x-ray diffraction patterns of these phases are distinct from the pattern of the residual sI phase, polycrystalline x-ray diffraction of the large unit cells yields many overlapping diffraction lines that hinder structure determination. Growing single crystals of the investigated phases is therefore key to unequivocal characterization. Here, we heated the sample to eliminate the sI phase (Fig. 2*b*) and brought the investigated phase to its melting/decomposition point to reduce numerous crystallites to several residual crystals (Fig. 2*c*). Under subsequent cooling, the seeds of the investigated phase grew into euhedral single crystals displaying a hexagonal platelet habit (Fig. 2*d*). When viewed through the edge (prism side) of the platelet, the optical birefringence under cross polarization clearly indicated a difference from the cubic (isotropic) sI phase (19). Repeating this heating–cooling process, we succeeded in growing a bulk hexagonal prism single crystal of the investigated phase (Fig. 2*e*) for x-ray diffraction.

In situ energy dispersive x-ray diffraction scans of the single crystal in the diamond cell (20) were performed at the superconducting wiggler beamline X17C of the National Synchrotron Light Source, Brookhaven National Laboratory. Single-crystal peaks were collected with an intrinsic germanium detector at $2\theta = 8°$ ($Ed = 88.87$ keV·Å). With two orthogonal rotation axes χ and ω as defined by crystallographic convention, the diamond cell was oriented to search for diffraction peaks (21). The ω rocking curves of the diffraction peaks were very sharp, typically within $\pm 0.1°$ of the ω angle at 25 keV, indicating a high-quality single crystal. With accurate determination of the χ–ω orientation of two diffraction planes, the orientation matrix was defined for orientations of other diffraction planes. Single-crystal x-ray diffraction provides unambiguous determination of structure as it resolves orientations in reciprocal space in addition to d-spacings. Overlapping lines in polycrystalline diffraction appear at entirely different points in χ–ω reciprocal space in single-crystal diffraction. Measurements of 79 diffraction peaks in 60 classes of the investigated phase of methane hydrate at 600 MPa (Fig. 2*e*) are refined to a hexagonal unit cell of $a = 11.980(2)$ Å, $c = 9.992(3)$ Å, and volume $V = 1241.9(5)$ Å^3. The structure is very similar to the known sH gas hydrate (space group $P6/mmm$, $a = 12.26$ Å, $c = 10.17$ Å) with a slight compression. Similarly, measurements of 222 diffraction peaks in 49 classes for the investigated phase crystals at 250 MPa (Fig. 2*f*) are refined to a cubic unit cell of $a = 17.158(2)$ Å and $V = 5051.3(13)$ Å^3. The structure is identical to the known sII gas hydrate (space group $Fd3m$, $a = 17.1$ Å), as the diffraction peaks follow exactly the

Abbreviations: sI, structure I; sII, structure II; sH, structure H.

†To whom reprint requests should be addressed. E-mail: imchou@usgs.gov.

‖Dyadin, Y. A. & Aladko, E. Y., Proceedings of the 2nd International Conference on Natural Gas Hydrates, June 2–6, 1996, Toulouse, France, pp. 67–70.

The publication costs of this article were defrayed in part by page charge payment. This article must therefore be hereby marked "*advertisement*" in accordance with 18 U.S.C. §1734 solely to indicate this fact.

Article published online before print: *Proc. Natl. Acad. Sci. USA*, 10.1073/pnas.250466497. Article and publication date are at www.pnas.org/cgi/doi/10.1073/pnas.250466497

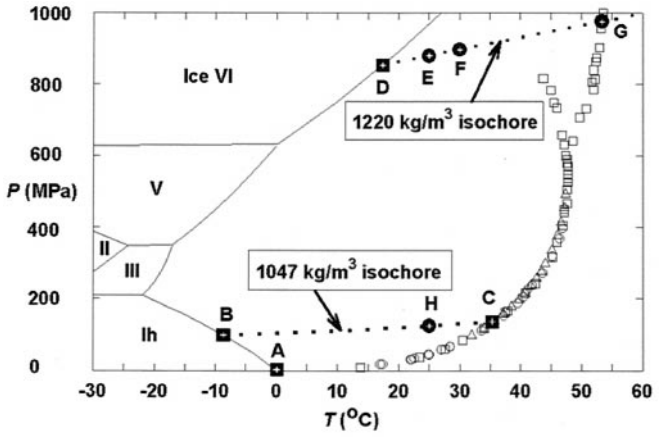

Fig. 1. Previous experimental results and the pressure–temperature (*P–T*) conditions for *in situ* observations in this study for the system CH_4–H_2O. The experimental data for the univariant *P–T* relations of the assemblage methane hydrate–water–methane vapor were taken from Marshall *et al.* (circles; ref. 10), Dyadin *et al.* (squares; ref. 11, ‖), and Nakano *et al.* (triangles; ref. 12). All symbols are for sI methane hydrate, except those squares branching out at higher *P–T* conditions. The boundaries for the stable ice phases and their melting curves (solid lines) are from ref. 13. Points A, B, C, and D (solid squares) indicate the *P–T* conditions for four invariant points, and they are for the following assemblages, respectively: sI methane hydrate–liquid water (Lw)–ice Ih–methane vapor (V), sI and sII methane hydrates–Lw–ice Ih, sI and sII methane hydrates–Lw–V, and sI and sH methane hydrates–Lw–ice VI. Points E, F, and G (dots) are *P–T* points along the isochore of pure water for 1,220 kg/m^3 (14), and point H (dot) is a *P–T* point along the isochore of pure water for 1,047 kg/m^3. The former isochore was defined by the melting *P–T* condition of ice VI at point D (16.6°C and 0.84 MPa; ref. 15), and the latter isochore by the melting *P–T* condition of ice Ih at point B (−8.7°C and 99 MPa; I-M.C., A.S., R.C.B., R.J.H., A.F.G., L.A.S., and S.H.K., unpublished observations). The latter isochore is also the univariant *P–T* conditions for the assemblage sI and sII methane hydrates–Lw (I-M.C., A.S., R.C.B., R.J.H., A.F.G., L.A.S., and S.H.K., unpublished observations).

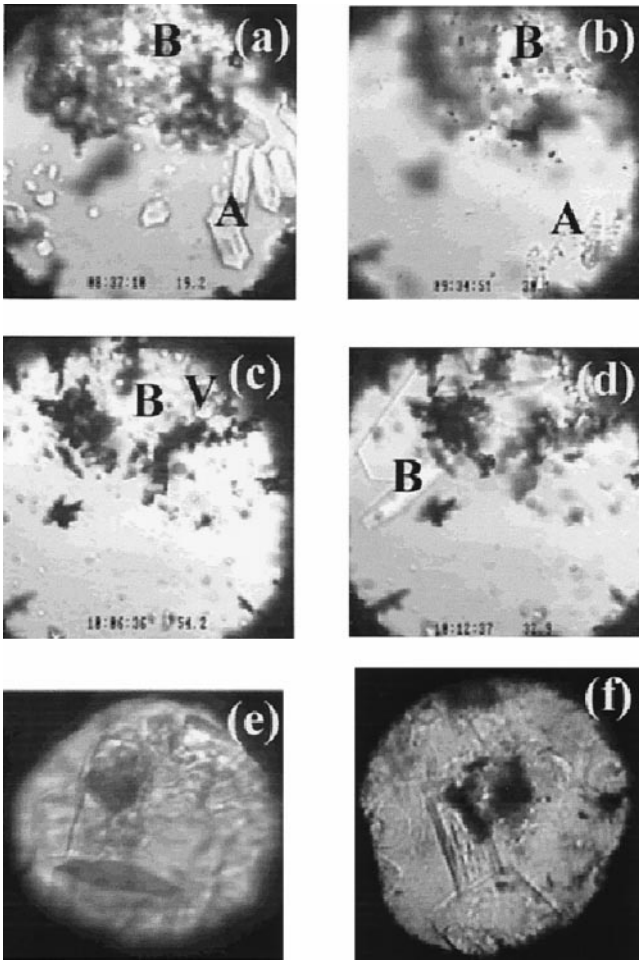

Fig. 2. (*a–d*) Images of a sample during a cooling, heating, and cooling cycle. (*a*) The coexistence of sI methane hydrate (A), sH methane hydrate (B), and water at 19.2°C and 880 MPa (near point D in Fig. 1). (*b*) The trace of sI methane hydrate at about 30°C and 900 MPa (point F in Fig. 1) immediately preceding full dissociation induced by heating. (*c*) The partial decomposition of the sH methane hydrate at 54°C and 980 MPa (point G in Fig. 1) and the formation of methane vapor (bubbles at the top-right corner indicated by V). (*d*) The growth of sH methane hydrate crystals during slow cooling at 33°C and 910 MPa (near point F in Fig. 1). (*e*) Images of single crystals of sH methane hydrate of a different sample at about 600 MPa and 25°C, taken after synchrotron x-ray diffraction analysis. The dark circular area is the spot damaged by the x-ray beam. The hexagonal dark area at lower part of the view is the base (001) face, and the hexagonal prism faces (100) are also clearly shown. (*f*) Images of single crystals of sII methane hydrate at about 250 MPa and 25°C, taken after synchrotron x-ray diffraction analysis. The dark circular area at the center of the view is the spot damaged by the x-ray beam. The cubic (100) face is clearly shown for the crystal at the lower part of the view. (The field of view in *a–d* is about 0.3 mm and the sample chamber is about 0.25 mm thick. The field of view in *e* and *f* is about 0.2 mm, and the sample is about 0.15 mm thick.)

extinction rules of *Fd3m*. Representative single-crystal energy dispersive x-ray diffraction patterns of the investigated methane hydrate phases are shown in Fig. 3. The results clearly verify the discovery of two phases of pure methane hydrate. After this work was completed, we learned of a polycrystalline neutron diffraction study of methane hydrate (J. S. Loveday, R. J. Nelmes, S. A. Belmonte, D. R. Allan, D. D. Klug, J. S. Tse, and Y. P. Handa, personal communication) that arrived at similar conclusions regarding the sH phase, but did not mention the sII.

With the structures identified, the characteristic Raman peaks can be used as a fingerprint for the three methane hydrate phases, and can be further used to reveal the occupancy of cavities. Fig. 4 compares the Raman spectra of methane hydrate in the three structure types, sI, sII, and sH. The unit cell of sI methane hydrate contains two 5^{12} cavities, six $5^{12}6^2$ cavities, and 46 H_2O molecules, with one CH_4 molecule in each cavity. The CH_4 ν_1 band in sI methane hydrate is a doublet at 2,904 and 2,915 cm^{-1}, with an intensity ratio of 3:1, indicating that the number of large cavities in a unit cell of the structure is 3 times that for the small cavities (22). The CH_4 ν_1 band for the sII phase is a doublet at 2,904 and 2,910 cm^{-1}, with an intensity ratio of about 1:2, indicating the number of large cavities in a unit cell of sII is half that for the small cavities. This is consistent with the composition of the sII of gas hydrates having sixteen 5^{12} cavities, eight $5^{12}6^4$ cavities, and 136 H_2O molecules, assuming each cavity contains one CH_4 molecule. The unit cell of sH of gas hydrate contains three 5^{12} cavities, two $4^35^66^3$ cavities, one $5^{12}6^8$ cavity, and 34 H_2O molecules. The two smaller cavities are easily filled by methane, but the $5^{12}6^8$ cavity is normally too large for methane; it would be necessary to put two or more methane molecules in this cavity to stabilize it, in a manner similar to the double-occupancy cage filling postulated for nitrogen hydrate between 100 and 250 MPa (23). As shown in Fig. 4, the Raman spectrum of sH methane hydrate is very different from the spectra for sI and sII. A deconvolved Raman spectrum of the ν_1 band of CH_4 in sH methane hydrate collected at 25°C and 880 MPa shows a doublet at 2,917 and 2,927 cm^{-1}, with a peak area ratio of about 3:1 (Fig. 4). Assignment of the two peaks to three cavities (with possible overlapping Raman

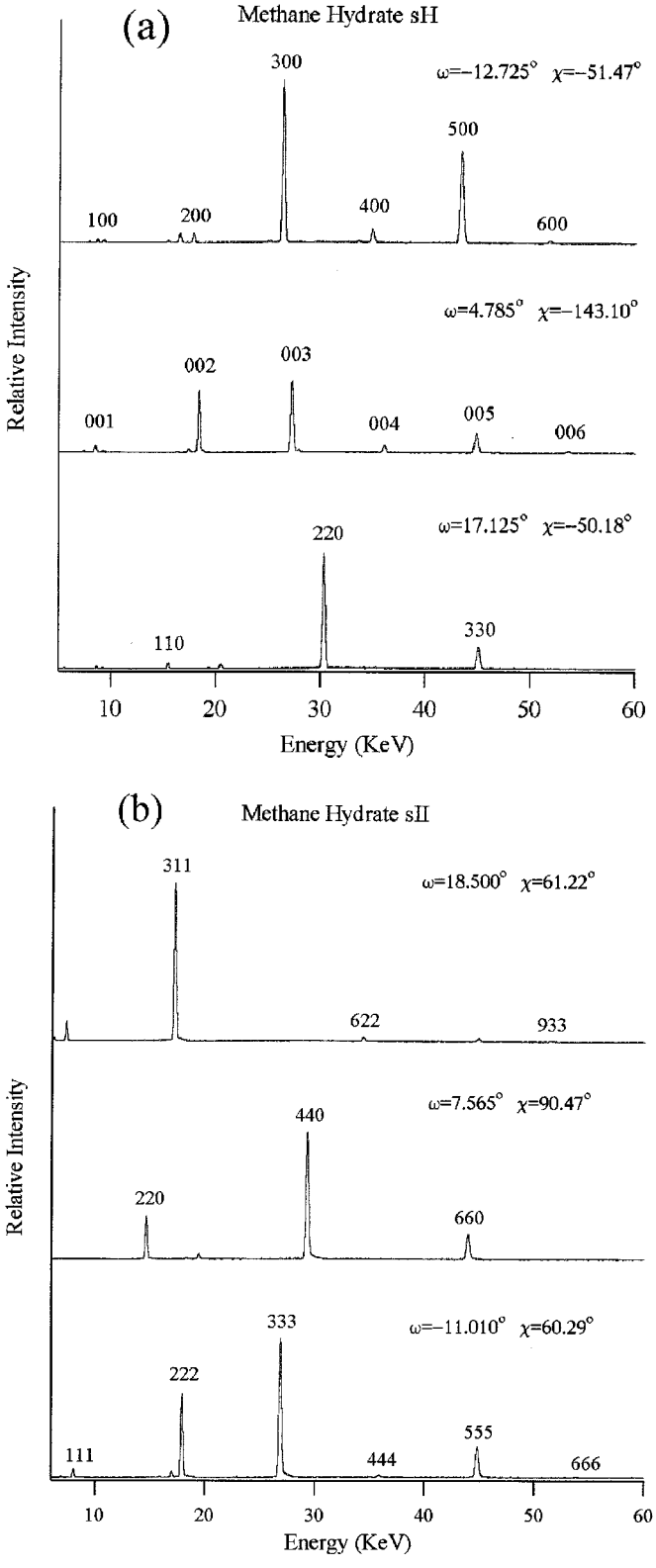

Fig. 3. Representative single-crystal energy dispersive x-ray diffraction patterns of the investigated methane hydrate phases. (*a*) Three orthogonal orientations of the sH crystal at 600 MPa; $2\theta = 8.027°$, $Ed = 88.569$ keV·Å. (*b*) First three diffraction lines of the sII crystal at 250 MPa; $2\theta = 8.004°$, $Ed = 88.828$ keV·Å. Overtones are observed up to 90 keV, but are shown only to 60 keV. Weak peaks appearing at noninteger positions are fluorescence or escape peaks due to the intense reflections.

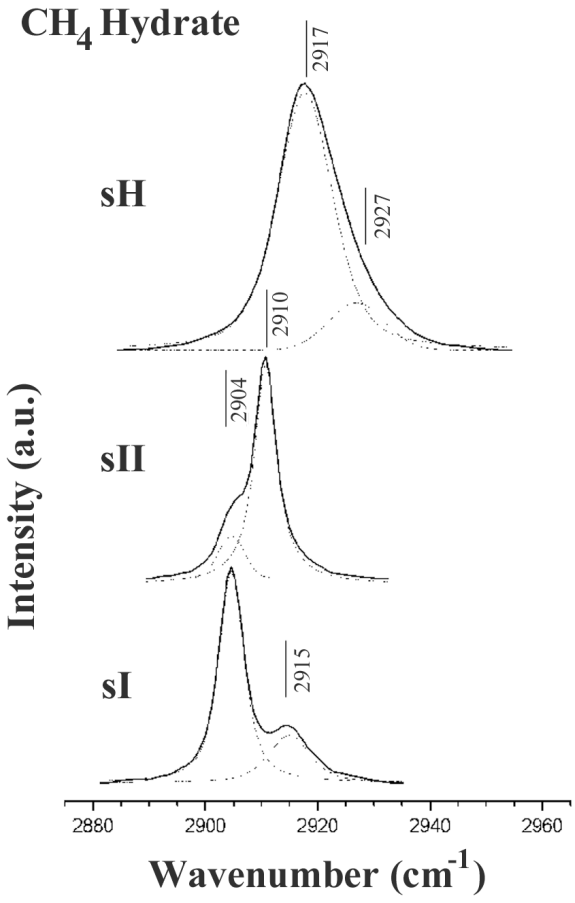

Fig. 4. Comparison of the Raman spectrum of the CH_4 ν_1 band of sH methane hydrate at 25°C and 880 MPa (point E in Fig. 1) with the spectra of sI and sII methane hydrates at 25°C and 125 MPa (point H in Fig. 1). a.u., Arbitrary units. Also shown in dashed lines are the spectral deconvolutions of these Raman spectra.

peaks) would require further investigation of the methane cavity occupancy.

The present study shows that upon compression, sI methane hydrate transforms to the sII phase at 100 MPa, and then the sH phase at 600 MPa. The implications to naturally occurring hydrates are far-reaching. The dominance of the sI methane hydrate in sediments of shallow continental shelves and permafrost areas will be taken over by sII at greater depth. The transformation caused by pressures at depths would be greatly favored with the presence of small quantities of ethane or propane in natural environments. The sII and sH methane hydrates are also likely to be major methane-bearing phases in the outer planets and their satellites (24, 25). Further investigation of their *P–T* stability, composition, cavity filling, and associations with other gas molecules will provide additional insight into these intriguing and ubiquitous materials in nature.

We thank the National Synchrotron Light Source for synchrotron beam time, and Paul B. Barton and Bruce S. Hemingway for constructive review. Work by I-M.C., L.A.S., and S.H.K. was partially supported by the Lawrence Livermore National Laboratory Gas Hydrates Program through its Laboratory Directed Research and Development Office. Work performed by A.S., J.F.S., H.-k.M., R.J.H., and A.F.G. was supported by the National Science Foundation Center for High-Pressure Research, the National Aeronautics and Space Administration Planetary Geology and Geophysics Program, and the National Aeronautics and Space Administration Astrobiology Institute.

1. Holbrook, W. S., Hoskins, H., Wood, W. T., Stephen, R. A. & Lizarralde, D. (1996) *Science* **273,** 1840–1843.
2. Petrenko, V. F. & Whitworth, R. W. (1999) *Physics of Ice* (Clarendon, Oxford).
3. Chou, I-M., Blank, J. G., Goncharov, A. F., Mao, H.-k. & Hemley, R. J. (1998) *Science* **281,** 809–812.
4. Dyadin, Y. A., Bondaryuk, I. V. & Zhurko, F. V. (1991) in *Inorganic and Physical Aspects of Inclusion*, Inclusion Compounds, eds. Atwood, J. L., Davies, J. E. D. & MacNicol, D. D. (Oxford Univ. Press, Oxford), Vol. 5, pp. 213–275.
5. Jeffrey, G. A. (1984) in *Inclusion Compounds,* eds. Atwood, J. L., Davies, J. E. D. & MacNicol, D. D. (Academic, London), Vol. 1, pp.135–190.
6. Ripmeester, J. A., Ratcliffe, C. I., Klug, D. D. & Tse, J. S. (1994) *Ann. N.Y. Acad. Sci.* **715,** 161–176.
7. Sloan, E. D., Jr. (1998) *Clathrate Hydrates of Natural Gases* (Dekker, New York), 2nd Ed.
8. Subramanian, S., Kini, R. A., Dec, S. F. & Sloan, E. D., Jr. (2000) *Chem. Eng. Sci.* **55,** 1981–1999.
9. von Stackelberg, M. & Jahns, W. (1954) *Z. Elektrochem.* **58,** 162–164.
10. Marshall, D. R., Saito, S. & Yashi, R. K. (1964) *AIChE J* **10,** 202–205.
11. Dyadin, Y. A., Aladko, E. Y. & Larionov, E. G. (1997) *Mendeleev Commun.* 34–35.
12. Nakano, S., Moritoki, M. & Ohgaki, K. (1999) *J. Chem. Eng. Data* **44,** 254–257.
13. Haselton, Jr., H. T., Chou, I.-M., Shen, A. H. & Bassett, W. A. (1995) *Am. Mineral.* **80,** 1302–1306.
14. Saul, A. & Wagner, W. (1989) *J. Phys. Chem. Ref. Data* **18,** 1537–1564.
15. Wagner, W., Saul, A. & Pruß, A. (1994) *J. Phys. Chem. Ref. Data* **23,** 515–527.
16. Hirai, H., Kondo, T., Hasegawa, M., Yagi, T., Yamamoto, Y., Komai, T., Nagashima, K., Sakashita, M., Fujihisa, H. & Aoki, K. (2000) *J. Phys. Chem. B* **104,** 1429–1433.
17. Stern, L. A., Kirby, S. H. & Durham, W. B. (1996) *Science* **273,** 1843–1848.
18. Bassett, W. A., Shen, A. H., Bucknum, M. & Chou, I. M. (1993) *Rev. Sci. Instrum.* **64,** 2340–2345.
19. Smelik, E. A. & King, H. E., Jr. (1997) *Am. Mineral.* **82,** 88–98.
20. Merrill, L. & Bassett, W. A. (1974) *Rev. Sci. Instrum.* **45,** 290–294.
21. Mao, H. K., Jephcoat, A. P., Hemley, R. J., Finger, L. W., Zha, C. S., Hazen, R. M. & Cox, D. E. (1988) *Science* **239,** 1131–1134.
22. Sum, A. K., Burruss, R. C. & Sloan, E. D., Jr. (1997) *J. Phys. Chem. B* **101,** 7371–7377.
23. Kuhs, W. F., Chazallon, B., Radaellie, P. G. & Pauer, F. (1997) *J. Inclusion Phenom. Mol. Recognit. Chem.* **29,** 65–77.
24. Lunine, J. I. & Stevenson, D. J. (1985) *Astrophys. J. Suppl. Ser.* **58,** 493–531.
25. Lunine, J. I. & Stevenson, D. J. (1987) *Icarus* **70,** 61–77.